Inorganic Chemistry

Article

Polar Symmetry and Intercalation of New Multilayered Hybrid Molybdates: $[M_2(pzc)_2(H_2O)_x][Mo_5O_{16}]$ (M = Co, Ni)

Bangbo Yan and Paul A. Maggard*

Department of Chemistry, 2620 Yarbrough Drive, North Carolina State University, Raleigh, North Carolina 27695-8204

The layered molybdate $[M_2(pzc)_2(H_2O)_x][Mo_5O_{16}]$ (**I**: M = Ni, x = 5.0; **II**: M = Co, x = 4.0; pzc = pyrazinecarboxylate) hybrid solids were synthesized via hydrothermal reactions at 160–165 °C. The structures were determined by single-crystal X-ray diffraction data for **I** (Cc, Z = 4; a = 33.217(4) Å, b = 5.6416(8) Å, c = 13.982(2) Å, β = 99.407(8)°, and V = 2585.0(6) Å^3) and powder X-ray diffraction data for **II** ($C2/c$, Z = 4; a = 35.42(6) Å, b = 5.697(9) Å, c = 14.28(2) Å, β = 114.95(4)°, and V = 2614(12) Å^3). The polar structure of **I** contains new $[Ni_2(pzc)_2(H_2O)_5]^{2+}$ double layers that form an asymmetric pattern of hydrogen bonds and co-valent bonds to stair-stepped $[Mo_5O_{16}]^{2-}$ sheets, inducing a net dipole moment in the latter. In **II**, however, the $[Co_2(pzc)_2(H_2O)_4]^{2+}$ double layers have one less coordinated water and subsequently exhibit a symmetric pattern of covalent and hydrogen bonding to the $[Mo_5O_{16}]^{2-}$ sheets, leading to a centrosymmetric structure. Thermogravimetric analyses and powder X-ray diffraction data reveal that **I** can be dehydrated and rehydrated with from 0 to 6.5 water molecules per formula unit, which is coupled with a corresponding contraction/expansion of the interlayer distances. Also, the dehydrated form of **I** can be intercalated by ~4.3 H$_2$S molecules per formula unit, but the intercalation by pyridine or methanol is limited to less than one molecule per formula unit.

Introduction

Layered solids continue to be an intense focus of research, owing to the diversity of applications which derive from their intercalation chemistry, such as those found in catalysts, battery electrodes, in separations, or in sensors.[1-3] Alternative perspectives on layered structures emphasize investigations of their low-dimensional electronic or magnetic properties, such as typified by charge or spin-driven electronic transitions.[4,5] Our efforts in these fields have been directed toward layered solids that can exhibit both intercalative and desirable electronic/magnetic properties and that can be targeted via the syntheses of multilayered or pillared metal-oxides/organics featuring a segregated heterometallic atom distribution. In these structures, the organic ligands preferentially coordinate to late transition metals to form metal-organic layers or pillars, which then additionally bond to the early transition metals of oxide layers. Examples include the layered vanadium oxides interleaved with $Cu(pyz)_2^{2+}$ (pyz = pyrazine) square nets or with $M(pyz)^{2+}$ (M = Co, Ni, Zn) layers of chains,[6,7] or the layered pillared perrhenates involving simple organic or $M(pzc)_2(H_2O)_{2-x}$ (M = Co, Ni, Cu; pzc = pyrazinecarboxylate) metal-coordinated pillars.[8-10] These heterometallic layered hybrids enable novel combinations of the intercalative/absorptive-type properties of layered solids, such as porosity and open metal sites, together with the expression of optical, electrical, and magnetic properties of low-dimensional structures. Further, their organic components allow for a wide range of functionality and possible structural modifications.

* To whom correspondence should be addressed. E-mail: Paul_Maggard@ncsu.edu.

(1) *Intercalation Chemistry*; Whittingham, M. S., Jacobson, A. J., Eds.; Academic Press: New York, 1982.
(2) *Pillared Layered Structures: Current Trends And Applications*; Mitchell, I. V., Ed.; Elsevier Applied Science, New York, 1990.
(3) *Inorganic Materials*; Bruce, D. W., O'Hare, D., Eds.; Wiley: Chichester, 1996.
(4) *New Horizons in Low-Dimensional Electron Systems*; Aoki, H., Tsukada, M., Schlüter, M., Lévy, F. A., Eds.; Kluwer Academic Publishers: Norwell, MA, 1991.
(5) *Strong Interactions in Low Dimensions*; Baeriswyl, D., Degiorgi, L., Eds.; Kluwer Academic Publishers: Norwell, MA, 1995.
(6) Maggard, P. A.; Boyle, P. D. *Inorg. Chem.* **2003**, *42*, 4250.
(7) Yan, B.; Luo, J.; Dube, P.; Sefat, A. S.; Greedan, J.; Maggard, P. A. *Inorg. Chem.* **2006**, submitted for publication.
(8) Lin, H.; Yan, B.; Boyle, P. D.; Maggard, P. A. *J. Solid State Chem.* **2006**, *179*, 39.
(9) Yan, B.; Capracotta, M. D.; Maggard, P. A. *Inorg. Chem.* **2005**, *44*, 6509.
(10) Maggard, P. A.; Yan, B.; Luo, J. *Angew. Chem., Int. Ed.* **2005**, *44*, 2553.

Hydrothermal synthetic techniques have contributed greatly to the growth and number of known hybrid oxides/organics in the vanadate, tungstate, and molybdate families.[11−17] Metal-oxide layers found in these hybrid structures are often related, or even isostructural, to those found in simpler inorganic solids. For example, in the molybdate family, a number of MoO_3-derived layers is known, some of which have been pillared by simple organics and investigated for their intercalative properties.[18−23] A representative system is $A_2Mo_nO_{3n+1}$ (A = alkali metal; n = positive integer) which features ReO_3-type molybdate layers with n number of corner-shared MoO_6 octahedra spanning the width of the layer. The $n = 5$ member contains a $[Mo_5O_{16}]^{2-}$ layer that was first reported in $Cs_2Mo_5O_{16}$[24] and also was recently hydrothermally synthesized within both $(C_2H_{10}N_2)[Mo_5O_{16}]$ and $(C_4H_{12}N_2)[Mo_5O_{16}]$.[25] The latter structures result from the replacement of interlayer Cs^+ for organic cations. These layered structures might be expected to exhibit microporosity or intercalative-type properties, though none have been reported. Thus, the hydrothermal synthesis of multilayered molybdate/metal-organics was investigated in order to explore different and new types of interlamellar bonding interactions in order to understand their effect on the structures and properties of the molybdate layers.

The syntheses of new multilayered molybdates containing $[Mo_5O_{16}]^{2-}$ layers and interlamellar $[M_2(pzc)_2(H_2O)_x]^{2+}$ (**I**: M = Ni, x = 5.0; **II**: M = Co, x = 4.0) double layers of chains are reported herein. The interlayer metal-oxide/organic interactions have been investigated for their role in inducing a net polarization in the $[Mo_5O_{16}]^{2-}$ layers for **I** but which are symmetric for **II**. Further, the activity of **I** toward small molecule intercalation has been tested for H_2O, H_2S, methanol, and pyridine. The employed characterization methods included powder and single-crystal X-ray diffraction, thermogravimetric analysis, and UV−vis diffuse reflectance.

Experimental Section

Materials. All starting materials were used as received from the chemical supplier, including MoO_3 (99.9995%), pyrazinecarboxylic acid (99%), $Co(OH)_2$ (99.9%+), and NiO (99.99%+). Reagent amounts of in-house deionized water were also used in the syntheses.

Synthesis. The hydrothermal synthesis of $[Ni_2(pzc)_2(H_2O)_5]$-$[Mo_5O_{16}]$ (**I**) was performed by combining nickel oxide (0.038 g, 0.52 mmol), pyrazinecarboxylic acid (0.064 g, 0.52 mmol), and molybdenum trioxide (0.186 g, 1.29 mmol) in deionized water (3.7 mL) in a 1:1:2.5:400 molar ratio. The reactants were heat-sealed inside FEP Teflon pouches. The Teflon pouches were then placed inside a Teflon-lined stainless steel reaction vessel that was backfilled with water (1/3 volume) before closing. This reaction vessel was heated inside a convection oven to 160 °C for 72 h, then to 165 °C for 48 h, and slowly cooled over 10 h to room temperature. Green-colored platelets were obtained in ∼70% yield based on the loaded stoichiometry, and these were filtered, washed, and dried at 40 °C. The product was single phase according to the powder X-ray diffraction data.

The synthesis of $[Co_2(pzc)_2(H_2O)_4][Mo_5O_{16}]$ (**II**) was performed according to similar procedures as described for **I** above, with the exception of replacing NiO with $Co(OH)_2$. The reactants were heated to 160 °C for 48 h and then slowly cooled to room temperature over 24 h. The products exhibited very thin platelet morphologies and were colored light orange/red. These platelets were found to be too small for a single-crystal X-ray analysis, and therefore, many different reaction conditions were tested to obtain more suitable crystals. However, longer reaction times of up to 240 h or higher reaction temperatures of up to 180 °C result in the conversion of these small platelets to $CoMo_4O_{13}(H_2O)_2$.[26] In addition, both shorter reaction times or lower temperatures yield unreacted starting materials. Thus, as **II** slowly transforms over time to an alternate phase, it appears to be a kinetic intermediate that can only be obtained as very small crystallites. The purity of **II** is >95% according to the powder X-ray diffraction data.

Single-Crystal Structure Determination. A single-crystal data set for **I** was collected at 293K on a Bruker-Nonius Apex2 CCD diffractometer using monochromatized Mo $K_{\alpha 1}$ radiation (λ = 0.71073 Å). The crystal was fixed on a 20-μm nylon loop with a small amount of immersion oil. The unit cell dimensions were determined from a symmetry-constrained fit of 2878 reflections for a 2θ range of 5.9−54.9°. The data collection employed a combination of ω and φ scans to collect data up to 2θ = 55.64°. The integration of frames was performed using SAINTPLUS[27] (12 410 total reflections, 5133 unique, R_{int} = 0.0365), and the raw data were corrected for absorption using SADABS.[28] The structure was solved and refined in the Bruker SHELXTL[29] software package in the monoclinic space group Cc, and the final space group assignment was confirmed using the software program PLATON.[30] Hydrogen atoms were introduced at idealized positions and were allowed to ride on the parent carbon positions. The structure refinement was performed using a full matrix least-squares based on F^2. The final least-squares cycle involved the anisotropic

(11) Zheng, L.-M.; Wang, X.; Wang, Y.; Jacobson, A. J. *J. Mater. Chem.* **2001**, *11*, 1100−1105.
(12) Devi, R. N.; Rabu, P.; Golub, V. O.; O'Connor, C. J.; Zubieta, J. *Solid State Sci.* **2002**, *4*, 1095−1102.
(13) Khan, M. I.; Yohannes, E.; Nome, R. C.; Ayesh, S.; Golub, V. O.; O'Connor, C. J.; Doedens, R. J. *Chem. Mater.* **2004**, *16*, 5273−5279.
(14) Shan, Y.; Huang, R. H.; Huang, S. D. *Angew. Chem., Int. Ed.* **1999**, *38*, 1751−1754.
(15) Liu, S.; Xie, L.; Gao, B.; Zhang, C.; Sun, C.; Li, D.; Su, Z. *Chem. Commun.* **2005**, 5023−5025.
(16) Rarig, R. S., Jr.; Lam, R.; Zavalij, P. Y.; Ngala, J. K.; LaDuca, R. L. Jr.; Greedan, J. E.; Zubieta, J. *Inorg. Chem.* **2002**, *41*, 2124−2133.
(17) Clemente-León, M.; Coronado, E.; Galán-Mascarós, J.-R.; Giménez-Saiz, C.; Gómez-Garcia, C. J.; Fernández-Otero, T. *J. Mater. Chem.* **1998**, *8(2)*, 309−312.
(18) Haber, J.; Lalik, E. *Catal. Today* **1997**, *33*, 119−137.
(19) Hosono, K.; Matsubara, I.; Murayama, N.; Woosuck, S.; Izu, N. *Chem. Mater.* **2005**, *17*, 349−354.
(20) Goward, G. R.; Kerr, T. A.; Power, W. P.; Nazar, L. F. *Adv. Mater.* **1998**, *10*, 449−452.
(21) Wei, X. M.; Zeng, H. C. *Chem. Mater.* **2003**, *15*, 433−442.
(22) Hagrman, P. J.; LaDuca, R. L., Jr.; Koo, H.-J.; Rarig, R., Jr.; Haushalter, R. C.; Whangbo, M.-H.; Zubieta, J. *Inorg. Chem.* **2000**, *39*, 4311.
(23) Xu, Y.; Lu, J.; Goh, N. K. *J. Mater. Chem.* **1999**, *9*, 1599.
(24) Gatehouse, B. M.; Miskin, B. K. *Acta Crystallogr.* **1975**, *B31*, 1293.
(25) Guillou, N.; Férey, G. *J. Solid State Chem.* **1999**, *147*, 240.
(26) Eda, K.; Uno, Y.; Nagai, N.; Sotani, N.; Chen, C.; Whittingham, M. S. *J. Solid State Chem.* **2006**, published online.
(27) *SAINT-Plus Ver. 6.22 Data Processing for SMART System*; Bruker Analytical X-ray Instruments, Inc.: Madison, WI.
(28) Sheldrick, G. M. *SADABS ver. 2.03, Software for Area Detector Absorptions and Other Corrections*; Bruker Analytical X-ray Instruments, Inc.: Madison, WI.
(29) Sheldrick, G. M. *SHELXTL NT ver. 6.10, Software Package for the Refinement of Crystal Structures*; Bruker Analytical X-ray Instruments, Inc.: Madison, WI.
(30) Spek, A. L. *PLATON−A Multipurpose Crystallographic Tool*; Utrecht University: Utrecht, The Netherlands. Spek, A. L. *Acta Crystallogr. A* **1990**, *46*, C34.

Table 1. Selected Crystal and Refinement Data for **I**[a]

empirical formula	$Ni_2(C_5N_2O_2)_2(H_2O)_5Mo_5O_{16}$
fw	1189.39
space group, Z	Cc, 4
a, Å	33.217(4)
b, Å	5.6416(8)
c, Å	13.982(2)
β, °	99.407(8)
V, Å³	2585.0(6)
μ (Mo Kα), mm⁻¹	3.893
d_{calc}, g cm⁻³	3.056
reflns (total)	12 410
data/ restraints/params	5133/2/421
GOF	0.997
final R1, wR2 [$I > 2\sigma(I)$][b]	0.030, 0.065

[a] Refined cell parameters for **II**, in $C2/c$, were $a = 35.42(6)$ Å, $b = 5.697(9)$ Å, $c = 14.28(2)$ Å, $\beta = 114.95(4)°$, and $V = 2614(12)$ Å³. [b] R1 $= \sum||F_o| - |F_c||/\sum|F_o|$; wR2 $= \{\sum[w(F_o - F_c)^2]/\sum[wF_o^2]\}^{1/2}$, $w = \sigma_F^{-2}$.

refinement of all non-H atoms and which converged to R1/wR2 = 0.0304/0.0652 and a GOF = 0.997 for 4393 reflections ($I > 2\sigma(I)$) and 421 parameters. The Flack parameter, which refined to 0.53(2), was indicative of racemic twinning. Some data collection and refinement parameters are given in Tables 1 and 2, and selected interatomic distances are compiled in Table 3.

Powder X-ray Diffraction. High-resolution powder X-ray diffraction (PXRD) data were collected in transmission mode on an INEL diffractometer using Cu Kα1 ($\lambda = 1.54056$ Å) radiation from a sealed-tube X-ray generator (35 kV, 30 mA) and a curved position-sensitive detector. All attempts at indexing the unit cell and refining the structure of **II** were performed using the software program GSAS.[31] During the refinements, the structural models that were tested included the noncentrosymmetric structure found for **I** and the known centrosymmetric $(C_4H_{12}N_2)[Mo_5O_{16}]$ structure.[25] The model with the best fit to the data, with wR$_p$/R$_p$ = 0.103/0.066, was found in the centrosymmetric space group $C2/c$ and yielded the formula $[Co_2(pzc)_2(H_2O)_4][Mo_5O_{16}]$. However, the precise atomic positions and thermal ellipsoids could not be refined, owing to the very high background and the asymmetric peak profiles. The unit cell refinement is given in the footnotes to Table 1, and additional refinement and structural details are available in the Supporting Information.

Bulk Characterization Techniques. Thermogravimetric analyses of **I** and **II** were taken on a TA Instruments TGA Q50 under flowing nitrogen at a heating rate of 5 °C/min. The UV–vis diffuse reflectance spectra (DRS) were taken on powdered samples mounted onto a fused-silica slide that was placed along the external window of an integrating sphere inside a Cary 300 spectrophotometer. A pressed poly(tetrafluoroethylene) powder was used as a reference, and the data were plotted as the remission function $F(R_\infty) = (1 - R_\infty)^2/(2R_\infty)$, where R is diffuse reflectance based on the Kubelka–Monk theory of diffuse reflectance.

Results and Discussion

Syntheses. The hydrothermal reaction of MoO_3, NiO, and pyrazinecarboxylate at 160–165 °C for 5 days yields greenish-blue crystals with the composition $[Ni_2(pzc)_2(H_2O)_5]$-$[Mo_5O_{16}]$ (**I**). However, an analogous synthetic procedure, except with the substitution of Co for Ni, results in light orange/red colored crystals that are unsuitable for single-crystal X-ray analysis. The PXRD data for the M = Co phase (**II**) show that it has a structure closely related to that of **I**,

(31) Larson, A. C.; Von Dreele, R. B. *General Structure Analysis System (GSAS)*; Los Alamos National Laboratory Report LAUR 86-748, 2000.

Table 2. Atomic Coordinates ($\times 10^4$) and Equivalent Isotropic Displacement Parameters (Å², $\times 10^3$) for **I**

atom	x	y	z	U(eq)[a]
Mo1	3117(1)	7033(1)	4021(1)	10(1)
Mo2	2187(1)	8279(1)	4346(1)	9(1)
Mo3	2512(1)	3585(1)	2544(1)	10(1)
Mo4	1921(1)	7201(1)	1082(1)	11(1)
Mo5	2861(1)	8354(1)	795(1)	10(1)
Ni1	4137(1)	4786(2)	4977(1)	13(1)
Ni2	5777(1)	10397(2)	2779(1)	13(1)
O1	4674(2)	9917(9)	3584(4)	23(1)
O2	4421(2)	7880(8)	4713(4)	18(1)
O3	5509(1)	7306(8)	3053(3)	16(1)
O4	5235(2)	5308(9)	4170(4)	21(1)
O5	3589(2)	6404(10)	4752(4)	17(1)
O6	2837(2)	8862(10)	4915(4)	11(1)
O7	3060(2)	4486(10)	3118(4)	12(1)
O8	3237(2)	9299(11)	3341(4)	19(1)
O9	2224(2)	10983(10)	5235(4)	12(1)
O10	2110(2)	6014(10)	5120(4)	17(1)
O11	1710(2)	8776(10)	3727(4)	15(1)
O12	2469(2)	6708(9)	3502(4)	14(1)
O13	2363(2)	1691(9)	3396(4)	14(1)
O14	1955(2)	4593(10)	1975(4)	12(1)
O15	2657(2)	1689(9)	1721(4)	11(1)
O16	2564(2)	6735(9)	1622(4)	10(1)
O17	1798(2)	9415(10)	1794(4)	18(1)
O18	1478(2)	6871(9)	260(4)	18(1)
O19	2928(2)	6153(10)	2(4)	15(1)
O20	3347(2)	8817(11)	1392(4)	19(1)
O1w	3876(2)	1565(9)	5068(4)	22(1)
O2w	4703(2)	3116(9)	5209(4)	21(1)
O3w	5198(2)	12003(10)	2529(3)	19(1)
O4w	5998(1)	13620(8)	2552(3)	16(1)
O5w	6347(2)	8799(8)	3064(4)	17(1)
N1	4153(2)	4873(10)	1506(4)	14(1)
N2	4101(2)	4615(10)	3466(4)	15(1)
N3	5786(2)	10693(10)	4289(4)	13(1)
N4	5753(2)	10317(10)	6267(4)	15(1)
C1	4312(2)	6320(12)	3115(4)	14(2)
C2	4348(2)	6442(15)	2147(6)	21(2)
C3	3925(2)	3230(12)	1847(5)	17(2)
C4	3902(2)	3074(13)	2833(5)	19(2)
C5	4490(2)	8177(12)	3850(5)	16(2)
C6	5587(2)	8918(12)	4639(5)	11(1)
C7	5568(2)	8737(13)	5609(5)	17(2)
C8	5954(2)	12074(12)	5926(5)	19(2)
C9	5971(2)	12280(13)	4925(5)	15(2)
C10	5427(2)	7025(12)	3918(5)	15(2)

[a] U(eq) is defined as one-third of the trace of the orthogonalized U_{ij} tensor.

but the asymmetric and broad peak widths are indicative of either structural disorder or smaller crystallite sizes. The PXRD data of **I** and **II** are shown in Figure 1a for comparison. As the water content of these layered structures is highly variable (see below thermogravimetric analysis (TGA) and PXRD data for **I** and **II**), the X-ray powder refinement and TGA results were together used to assign the chemical formula of **II** as $[Co_2(pzc)_2(H_2O)_4][Mo_5O_{16}]$. However, **II** appears to be a kinetic intermediate because it slowly transforms over longer reaction times to $CoMo_4O_{13}$-$(H_2O)_2$.[26] Synthetic attempts in alternative organic solvents were unsuccessful.

Structural Description. The structure of $[Ni_2(pzc)_2$-$(H_2O)_5][Mo_5O_{16}]$, shown in Figure 2 down the c axis, consists of molybdate $[Mo_5O_{16}]^{2-}$ layers with double layers of $[Ni_2(pzc)_2(H_2O)_5]^{2+}$ chains in the interlamellar regions. The $[Mo_5O_{16}]^{2-}$ layers stack down the a axis and are constructed from vertex-shared MoO_6 octahedra to give a ReO_3-type slab that is five octahedra wide and one octahedron thick. Each

Table 3. Selected Interatomic Distances (Å) and Bond Valence Sums[a] for **I**

atom	atom	distance, Å	atom	atom	distance, Å	atom	atom	distance, Å
Mo1	O5	1.764(6)	Mo3	O7	1.934(6)	Mo5	O6	1.989(5)
	O6	1.967(5)		O12	2.231(5)		O9	2.167(5)
	O7	1.901(5)		O13	1.731(5)		O15	2.442(5)
	O8	1.680(6)		O14	1.973(5)		O16	1.876(6)
	O12	2.164(6)		O15	1.698(5)		O19	1.704(5)
	O19	2.405(5)		O16	2.219(5)		O20	1.710(6)
	ΣS_{ij} =	5.96		ΣS_{ij} =	5.99		ΣS_{ij} =	6.06
Mo2	O6	2.201(5)	Mo4	O9	1.963(5)			
	O9	1.959(6)		O10	2.403(6)			
	O10	1.720(6)		O14	1.920(5)			
	O11	1.698(6)		O16	2.161(6)			
	O12	1.849(6)		O17	1.688(5)			
	O13	2.463(5)		O18	1.722(6)			
	ΣS_{ij} =	6.14		ΣS_{ij} =	6.06			
Ni1	O2	2.047(5)	Ni2	O3	2.023(5)			
	O5	2.012(6)		O3w	2.104(5)			
	O1w	2.025(5)		O4w	2.006(5)			
	O2w	2.081(5)		O5w	2.074(5)			
	N1	2.139(6)		N3	2.113(6)			
	N2	2.098(6)		N4	2.141(6)			

[a] $S_{ij} = e^{[(R_o - R)/B]}$, $B = 0.37$, $R_o = 1.908$ for Mo(VI).[32,33]
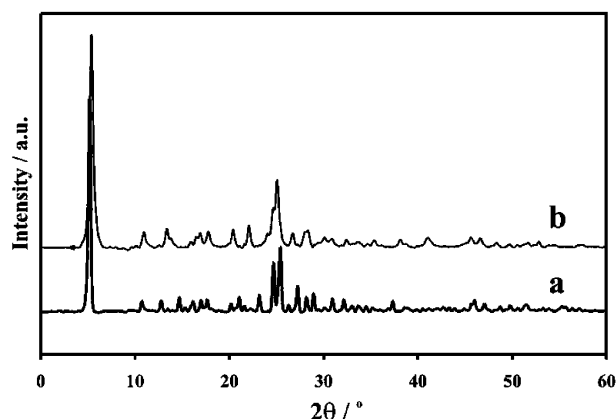
Figure 1. Powder X-ray diffraction patterns of $[M_2(pzc)_2(H_2O)_x][Mo_5O_{16}]$ for **I** (a, M = Ni) and **II** (b, M = Co).
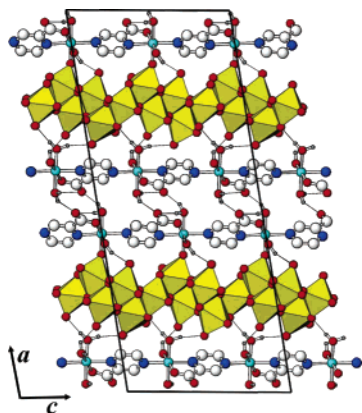
Figure 2. ~[010] view of the $[Ni_2(pzc)_2(H_2O)_5][Mo_5O_{16}]$ layered structure with the unit cell outlined. Red atoms = O, light blue = Ni, dark blue = N, white = C, and yellow polyhedra = MoO_6.

5×1 ReO_3-type slab is condensed via octahedral edges to identical neighboring 5×1 slabs which are overlayed by two and a half octahedra to form a stair-stepped sheet. The bond lengths around each MoO_6 octahedron, listed in Table 3, occur in a distinctive pattern and within the expected range for two long (2.161–2.463 Å), two medium (1.849–1.989

Å), and two short (1.680(6)–1.764(6) Å) Mo–O contacts and are consistent with prior known molybdate structures.[24,25] The calculated bond valence sums are listed in Table 3 and confirm the assignment of a Mo^{6+} oxidation state. Six symmetry-unique Mo atoms are located within each molybdate layer, Figure 3. The number of vertex-shared oxygen on each MoO_6 ranges from all shared for Mo3 (i.e., none are terminal), one terminal oxygen vertex for Mo2 and Mo5, and two terminal oxygen vertexes for Mo1 and Mo4. The terminal oxygen vertexes of the MoO_6 octahedra are located near the edges of the molybdate sheet. This layer is similar in structure to that of $Cs_2Mo_5O_{16}$ but with the addition of a small structural distortion that destroys a previous inversion relation between the Mo2/Mo5 and Mo1/Mo4 pairs.

The $[Ni_2(pzc)_2(H_2O)_5]^{2+}$ double layers are a remarkable structural feature of **I** that both lead to its polar symmetry and also regulate its intercalation chemistry. Two types of Ni–pzc chains occur, $[Ni(pzc)(H_2O)_2]^{1+}$ and $[Ni(pzc)(H_2O)_3]^{1+}$, and stack in layers oriented in opposite directions between the molybdate sheets. Both types of chains can be compared in either Figure 2 or Figure 4. Each Ni^{2+} is chelated by a nitrogen and oxygen on one side of the pzc ligand and is also coordinated (trans) to a lone nitrogen atom on a second ligand, Figure 4. The orientation of the pzc ligand is twisted by 67.4(2)° for Ni2 and 73.8(2)° for Ni1, and the chains deviate from linearity owing to the chelation of the ligand. The three remaining coordination sites on each Ni^{2+} are in a mer configuration. In the Ni2 chain (Figure 4b), these sites are bonded to three water molecules at 2.104(5), 2.023(5), and 2.006(5) Å to give $[Ni(pzc)(H_2O)_3]^{1+}$. For the Ni1 chain (Figure 4a), two of the mer sites are bonded to water molecules at 2.025(5) and 2.081(5) Å to give $[Ni(pzc)(H_2O)_2]^{1+}$. Both the Ni1 and Ni2 chains form hydrogen bonds to neighboring chains within the bc plane via the coordinated water and carboxylate groups at distances of ~2.8–2.9 Å for $OH_2\cdots O$ (between O1W–O4W and O1–O4). These two layers are also hydrogen bonded to each other and form the double-layer (O2W–H⋯O4 and O3W–H⋯O1 at 2.758(8) and 2.726(8) Å, respectively), drawn as thin lines in Figure 2. The remaining coordination site on Ni1 is bonded to the $[Mo_5O_{16}]^{2-}$ layer, Ni1–O5 at 2.012(6) Å, while the equivalent site on Ni2 is coordinated to a water molecule. Therefore, the $[Ni_2(pzc)_2(H_2O)_5]^{2+}$ double layer is coordinated to the $[Mo_5O_{16}]^{2-}$ layer through an asymmetric pattern of Ni–O and Ni–OH$_2$ hydrogen bonds for $[Ni(pzc)(H_2O)_2]^{1+}$ (Ni1) or solely Ni–OH$_2$ hydrogen bonds for $[Ni(pzc)(H_2O)_3]^{1+}$ (Ni2). The asymmetric Ni–O bonds of the $[Ni_2(pzc)_2(H_2O)_5]^{2+}$ layers align down the a axis and result in the polar space group Cc rather than C2/c as found for $Cs_2Mo_5O_{16}$.

The tentative structure of **II**, Figure 5, consists of $[Mo_5O_{16}]^{2-}$ molybdate layers separated by $[Co_2(pzc)_2(H_2O)_4]^{2+}$ double layers of chains. In contrast to **I**, the Co atoms in the double layers are now symmetry equivalent because each is coordinated to two water molecules and to the $[Mo_5O_{16}]^{2-}$ layer through one Co–O bond. Thus, the structure of **II** may be viewed as arising from **I** with the loss of one coordinated water molecule on the Ni2 chain.
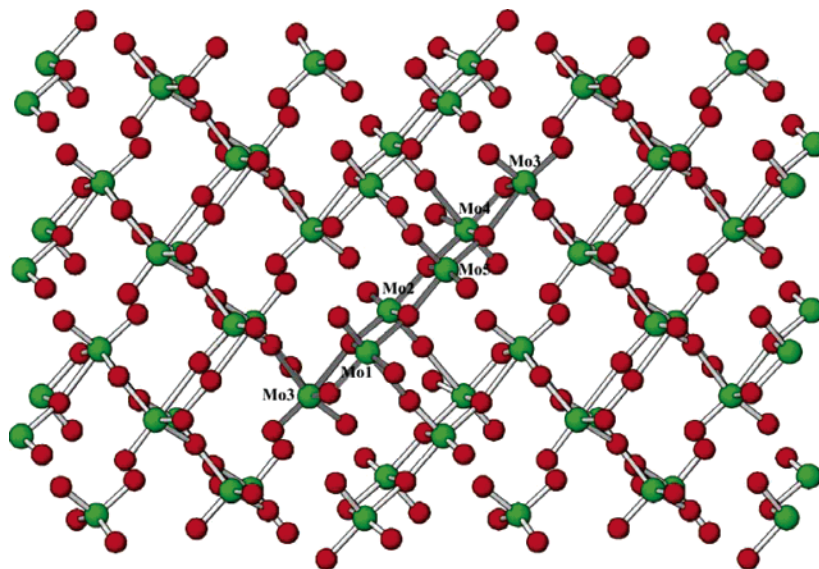
Figure 3. Structural view perpendicular to the $[Mo_5O_{16}]^{2-}$ layers in **I**. Red atoms = O and green atoms = Mo.
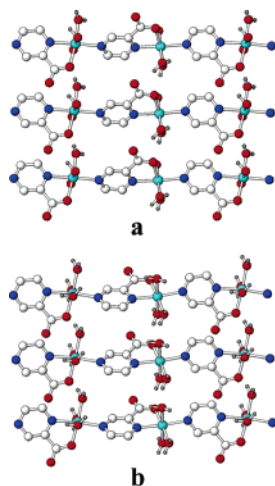

Figure 4. Structural view perpendicular to the two types of Ni−pzc layers, (a) $[Ni(pzc)(H_2O)_2]^+$ and (b) $[Ni(pzc)(H_2O)_3]^+$. Red atoms = O, light blue = Ni, dark blue = N, and white = C.

Figure 5. ~[010] view of the structural model for the centrosymmetric structure of **II**, $[Co_2(pzc)_2(H_2O)_4[Mo_5O_{16}]$. The unit cell is outlined and the red atoms = O, light blue = Ni, dark blue = N, white = C, and yellow polyhedra = MoO_6.

This structural change leads to a symmetric Co−O bonding pattern on both sides of the $[Mo_5O_{16}]^{2-}$ layer. Or alternatively, the intercalation of an additional water molecule from **II** to **I** occurs in an asymmetric fashion. These basic structural features are generally confirmed in the model obtained from powder X-ray data, but the precise interatomic distances and thermal ellipsoids cannot be determined, owing to some structural disorder and the variable water content (below).

While the $[Ni_2(pzc)_2(H_2O)_5]^{2+}$ chains, described above, are clearly asymmetric in their bonding to the $[Mo_5O_{16}]^{2-}$ layer, it is not obvious if any net dipole moment is induced across the $[Mo_5O_{16}]^{2-}$ layer itself. Local dipole moments of the MoO_6 octahedra were calculated for both $Cs_2Mo_5O_{16}$ and **I** using a combination of the well-known Debye equation ($\mu = neR$) and the charge assignments obtained from bond valence sums.[35] The results are compiled in Table 4. Absolute
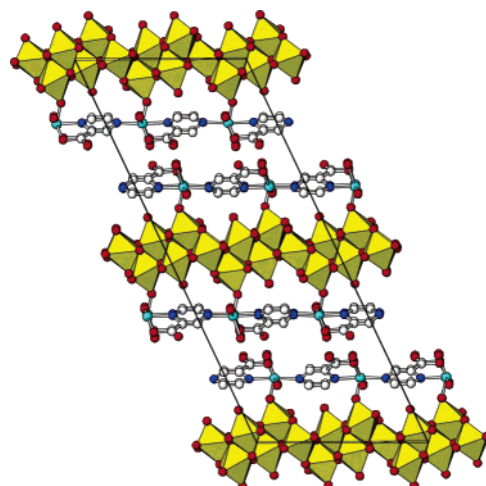
Table 4. Calculated Local Dipole Moments for Each MoO_6 Octahedra in $Cs_2Mo_5O_{16}$ and **I**, Together with the Hydrogen Bonding Interactions for Each[a]

$Cs_2Mo_5O_{16}$		$[Ni_2(pzc)_2(H_2O)_5][Mo_5O_{16}]$		
site	MoO_6 dipole[b]	equiv site	MoO_6 dipole[b]	H-bonds to MoO_6, Å
Mo1	6.63	Mo3	6.78	1.83
Mo2	7.77	Mo1	7.00	2.31, 1.76 (Ni−O)
		Mo4	7.41	1.88, 2.23, 2.13
Mo3	8.03	Mo2	8.35	1.90
		Mo5	8.47	1.88
		net moment: −5.16 (x axis), 1.29 (z axis)		

[a] Calculated for each local MoO_6 octahedron according to ref 35. [b] Dipole moments are given in units of debye (10^{-18} esu cm).

values of the dipole moments should be viewed with caution here, but their relative sizes show a clear relationship to the number of interlayer hydrogen bonds and Ni−O bonding

(32) Brown, I. D.; Altermatt, D. *Acta Crystallogr. B* **1985**, *41*, 244−247; Brese, N. E.; O'Keefe, M. *Acta Crystallogr. B* **1991**, *47*, 192−197.
(33) Hormillosa, C. *Bond Valence Calculator*, Version 2.00; McMaster University: Hamilton, Canada, 1993.
(34) Wessels, A. L.; Jeitschko, W. *J. Solid State Chem.* **1997**, *128*, 205−208.
(35) Maggard, P. A.; Nault, T. S.; Stern, C. L.; Poeppelmeier, K. R. *J. Solid State Chem.* **2003**, *175*, 27.

interactions. The Mo1- and Mo4-centered MoO_6 octahedra, which are related by inversion symmetry in $Cs_2Mo_5O_{16}$, participate in the largest number of interlayer hydrogen bonds and a Ni−O bond. Also, both Mo1 and Mo4 exhibit a significant reduction in their dipole moments compared to the equivalent site (Mo2) in $Cs_2Mo_5O_{16}$ (i.e., 7.77 D in $Cs_2Mo_5O_{16}$ vs 7.00 and 7.41 D in **I**; D = 10^{-18} esu cm). For Mo2, Mo3, and Mo5, which are located more internally within the layer and have a single hydrogen-bonding interaction, a larger MoO_6 dipole moment is observed (i.e., 6.78, 8.35, and 8.47 D for Mo3, Mo2, and Mo5 in **I** vs 6.63 and 8.03 D for Mo1 and Mo3 in $Cs_2Mo_5O_{16}$). Note the relatively small difference in dipole moments between Mo2 and Mo5 compared to much larger difference shown above between Mo1 and Mo4, Table 4. The net dipole moment of the $[Mo_5O_{16}]^{2-}$ layer in **I** is calculated to be −5.16 and 1.29 D down the x axis and z axis, respectively, while in $Cs_2Mo_5O_{16}$ there is no net dipole moment. Thus, the equivalent of approximately one asymmetric MoO_6 octahedron per formula unit does not self-cancel. These results are consistent with the space group symmetries of each, as the space group Cc for **I** restricts the dipole moment to lie within the ac plane, while the space group $C2/c$ for $Cs_2Mo_5O_{16}$ disallows a net overall dipole moment.

Optical Properties. The UV−vis diffuse reflectances of both **I** and **II** were measured to characterize their optical absorption wavelengths and are provided in the Supporting Information. The optical band gaps, extrapolated from the linear rise in absorption, occur at ∼420 nm or 2.95 eV for **I** and ∼430 nm or 2.88 eV for **II**. In previously reported molybdates, this optical absorption originates from a ligand-to-metal charge transfer between O^{2-} and Mo^{6+} that is typically around 2.8 eV.[36] The absorptions by the d−d transitions are weaker and are centered around 480 nm for **II**, and a very weak and broad absorption is centered around 650 nm for **I**. The absorption wavelengths are confirmed by their complementary red and blue crystal colors, respectively. Powdered samples of both **I** and **II** were also screened for second harmonic generation, but no activity was detected down to ∼50% of the SiO_2 signal. However, the tentative structural model for **II** is centrosymmetric and the intense sample colors suggests they might likely absorb much of the frequency-doubled light.

Thermogravimetric Analyses. The structures of both **I** and **II** contain relatively large amounts of water coordinated to the late transition metals. The TGA plot of **I**, Figure 6, shows a weight loss at ∼225−250 °C that corresponds with the removal of five coordinated water molecules per formula unit (obsd 7.8%, calcd 7.6%), in agreement with the composition. The TGA product after this step is a dehydrated layered structure of **I**, as described in the next section. A second broad weight loss occurs at ∼350−500 °C, corresponding to the decomposition of the organic ligand and concomitant reduction of Ni^{2+} and $[Mo_5O_{16}]^{2-}$ to Ni and MoO_2 (obsd 27.4%, calcd 28.8%). The latter products were identified via PXRD data of the TGA residues and given in
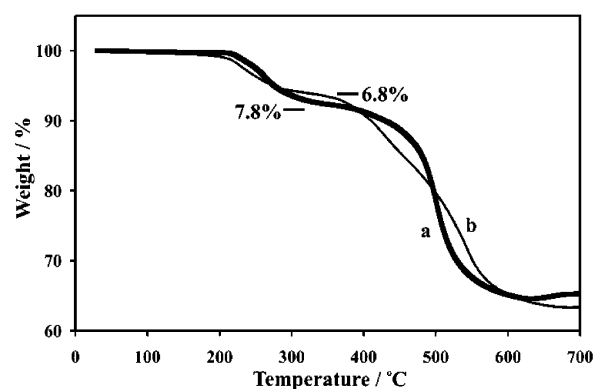
(36) Zhang, H. J.; Boutinaud, P.; Garcia, A.; Chaminade, J. P.; Fouassier, C. *Solid State Comm.* **1993**, *85*, 1031.

Figure 6. The thermogravimetric analysis of **I** (a) and **II** (b) plotted as wt % versus temperature.
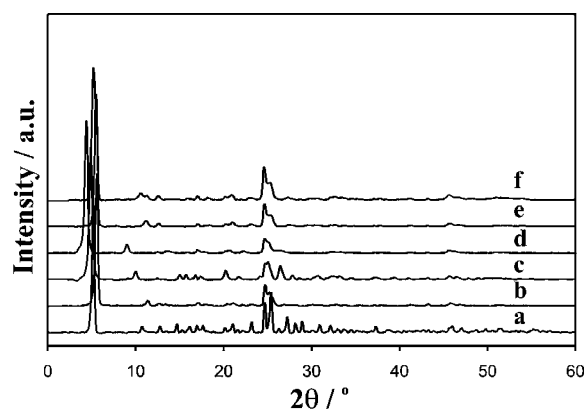

Figure 7. Powder X-ray diffraction patterns of **I** as synthesized (a), and after dehydration (b), rehydration (c), and intercalation by H_2S (d), methanol (e), and pyridine (f).

the Supporting Information. The molybdate layer is likely reduced by a reaction with the organic ligand, as investigated previously using tandem MS/TGA techniques in hybrid vanadate structures.[7] In the temperature range of ∼225−250 °C, a weight loss of ∼6.8% occurs similarly for **II**, but which is slightly higher than that expected for the removal of approximately four water molecules per formula unit (calcd 6.1%). However, **II** has a large possible range in water content, as investigated for **I** (below). Thus, the compositions of both **I** and **II** are dependent upon the sample preparation and history.

Small Molecule Intercalation. The layered structure of $[Ni_2(pzc)_2(H_2O)_5][Mo_5O_{16}]$ suggested that the intercalation of small molecules into the interlamellar regions might be possible. Further, the complete dehydration of **I** can be accomplished by heating under flowing N_2 at 230 °C for 3 h, resulting in a weight loss of 7.5% (calcd 7.6%) and a change in color from cyan to grass green. The PXRD patterns of both the original and dehydrated forms of **I**, Figure 7a and b, show a first intense diffraction peak for the interlayer (200) d-spacing at 16.39 and 15.13 Å, respectively. Table 5 lists the interlayer d-spacings for the dehydrated structure of **I**, as well as all intercalated products. Upon water removal, the interlayer distance contracts by ∼1.2 Å and the higher-angle diffraction peaks are both weaker and broader. The latter likely arises from packing disorder between the layers. When the dehydrated sample of **I** is soaked in water for a

Table 5. Interlayer (200) *d*-Spacings of **I** before and after the Intercalation of Guest Molecules*[a]*

compound **I**	2θ, deg	*d*(200), Å
as synthesized	5.389	16.39
dehydrated	5.836	15.13
rehydration	5.124	17.23
H$_2$S	4.612	19.14
methanol	5.720	15.44
pyridine	5.418, 5.744	16.30, 15.37

[a] The data are derived from the first intense reflections in Figure 7.
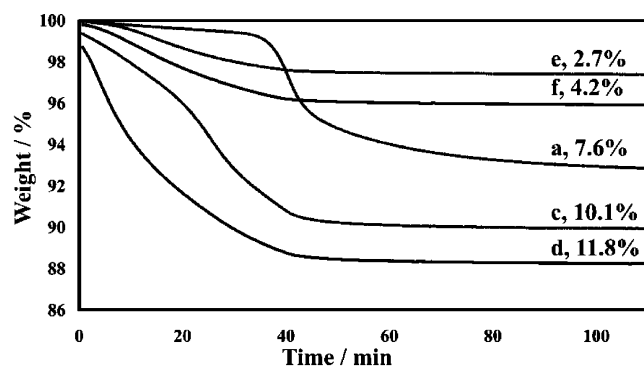
Figure 8. Thermogravimetric analysis at 230 °C for **I** (a), and after intercalation of the dehydrated structure by H$_2$O (c), H$_2$S (d), methanol (e), and pyridine (f). The labeling has been kept consistent with Figure 7.

few minutes, the sample color changes back to cyan to give a rehydrated compound. The PXRD pattern, Figure 7c, shows the (200) diffraction peak is shifted to a lower angle and that the interlayer spacing has increased by ∼0.8 Å compared to **I**. The TGA data of the rehydrated sample, Figure 8c, exhibit a 10.1% weight loss that is consistent with the removal of ∼6.5 water molecules per formula unit. The resulting formula for the rehydrated sample is [Ni$_2$(pzc)$_2$-(H$_2$O)$_{6.5}$][Mo$_5$O$_{16}$]. Further, **I** can be cycled between the fully dehydrated and rehydrated states with from 0 to ∼6.5 water molecules per formula unit. However, the structural organization and bonding of the interlayer water molecules must be somewhat changed in order to accommodate the extra ∼1.5 water molecules compared to **I**. A possible mechanism is the reversible insertion of H$_2$O into either the Ni−O (to MoO$_6$) or OH$_2$···O (to carboxylate groups) bonds of **I**. Similar dehydration/rehydration experiments for **II** were not investigated, owing to the lack of a fully refined structure for use in evaluating the data.

Alternative small molecule guests, including H$_2$S, methanol, and pyridine, were tested for their intercalation into the dehydrated form of **I**. The dehydrated sample was exposed to the guest molecules at room temperature by soaking for ∼20 h in either methanol or pyridine or by placing it in an atmosphere of H$_2$S for 17 h. The PXRD and TGA data of the products are shown in Figure 7d−f and Figure 8d−f. The calculated (200) *d*-spacings are listed in Table 5. After the dehydrated sample was placed in an H$_2$S atmosphere, its color changed to gray-blue and the PXRD data revealed a large increase in the interlayer *d*-spacing to 19.14 Å. The TGA results on the intercalated product, Figure 8d, show a weight loss (∼11.8%) consistent with the removal of ∼4.3 H$_2$S molecules per formula unit. The structural organization

of H$_2$S in the interlayer region of **I** is likely similar to that for H$_2$O, as it can both coordinate to the Ni sites and (more weakly) hydrogen bond to the [Mo$_5$O$_{16}$]$^{2-}$ layers. By comparison, the intercalation of methanol into **I** was relatively limited. The product exhibited a very small shift in its interlayer spacing to 15.44 Å and showed a small subsequent weight loss (∼2.7%) that was consistent with ∼1 intercalated methanol molecules per formula unit. Methanol will not coordinate very well to Ni^{2+} under these aqueous conditions, and as well, its limited ability to participate in hydrogen bonds may prohibit its uptake into the interlayer spaces. Pyridine also shows relatively limited intercalation into the structure, though it has been found to coordinate readily to Ni^{2+}. The pyridine-intercalated product exhibited two different interlayer *d*-spacings at 16.30 and 15.37 Å. The splitting of this main diffraction peak indicates that the intercalation by pyridine either is not complete or that a new structure is forming. The TGA results on the products show a small weight loss (∼4.2%) consistent with ∼0.6 pyridine molecules being removed on average per formula unit. The diffusion of pyridine into the interlayer spaces may be restricted, owing to its larger size. Thus, the intercalation of **I** shows a clear preference for smaller molecules that can participate in hydrogen bonding, as well as coordinate to Ni^{2+}, and which is reflected in the types of available bonding interactions within the interlayer spaces.

Conclusions

The new multilayered hybrid molybdates, [M$_2$(pzc)$_2$-(H$_2$O)$_x$][Mo$_5$O$_{16}$] (**I**: M = Ni; **II**: M = Co) contain [Mo$_5$O$_{16}$]$^{2-}$ layers that alternate in stacking with metal−organic [M$_2$(pzc)$_2$(H$_2$O)$_x$]$^{2+}$ double layers of chains. The noncentrosymmetric structure of **I** is induced by an asymmetric pattern of covalent and hydrogen bonding of the [Ni$_2$(pzc)$_2$(H$_2$O)$_5$]$^{2+}$ layers to the [Mo$_5$O$_{16}$]$^{2-}$ sheets. However, the structure of **II** is centrosymmetric, owing to the loss of one water molecule per formula to yield [Co$_2$(pzc)$_2$-(H$_2$O)$_4$]$^{2+}$ layers. The structure of **I** can be fully dehydrated and rehydrated up to a maximum of ∼6.5 water molecules per formula unit. The dehydrated form of **I** also absorbs up to ∼4.3 H$_2$S molecules per formula unit. However, neither methanol nor pyridine show appreciable intercalation into the dehydrated structure, owing to their larger sizes and weaker hydrogen bonding. The structures of these multilayered hybrids enable a new and dynamic way to couple intercalation selectivity with the physical properties that arise from noncentrosymmetric solids. Further research is underway on the synthesis of new solids containing these interesting [M$_2$(pzc)$_2$(H$_2$O)$_x$]$^{2+}$ double layers.

Supporting Information Available: Crystallographic data in CIF format and PXRD data of the TGA products. This material is available free of charge via the Internet at http://pubs.acs.org.

IC060253E